AFM nanoscale indentation in air of polymeric and hybrid materials with highly different stiffness

Raffaella Suriano*, Caterina Credi, Marinella Levi, Stefano Turri

Department of Chemistry, Materials and Chemical Engineering "Giulio Natta", Politecnico di Milano, Piazza Leonardo da Vinci 32, 20133 Milan, Italy

Article history:
Received 17 January 2014
Received in revised form 16 May 2014
Accepted 17 May 2014
Available online 24 May 2014

1. Introduction

The nanomechanical characterization of biological materials [1–8], thin rigid films [9–16] and soft matters [17–28] has been becoming increasingly important over the last two decades, because these materials are often too soft, fragile, inhomogeneous, or simply too small to be characterized through conventional, large scale mechanical tests. Nanoindentation is a suitable technique to analyze the local mechanical properties of very small, soft or thin samples [29–32]. Among the nanomechanical testing techniques, an atomic force microscope (AFM) can be used as a nanoindenter to obtain force–distance curves by applying very low loads in order to obtain small indentation depths. When force–distance curves are performed, an AFM probe is used as a nanoindentation tool, allowing the determination of elastic modulus of materials at the nanoscale By employing AFM for nanoindentations, the possible damage of delicate samples like living cells or hydrogels can be avoided [1,2,6] and local mechanical measurements with a nanoscale lateral resolution can be performed on finely featured samples [29]. Recently, the atomic force microscopy (AFM) has found increasingly wide applicability to investigation of mechanical properties of synthetic and biological samples. A greater understanding of the appropriate probe in terms of cantilever spring constant and tip shape as well as of the suitable theoretical model to be employed depending on samples examined during AFM indentation experiments is essential to achieve a good and reliable estimation of Young's modulus.

AFM probes are manufactured with different spring constants and tip shapes, and their surfaces can also be functionalized to optimize the experimental protocol for the specific sample to be analyzed. On the other side, this technique is sensitive to the adhesive forces occurring between the sample and the probe due both to the atomic interactions and the presence of an aqueous meniscus [33–36]. To minimize these effects, AFM nanoindentations are often carried out in an aqueous environment [1,6,7,17,20,25], even if this method can have some disadvantages like the difficult setting of the laser on the cantilever, and the disturbed signal on the photodiode due to the refraction effects given by the water–air interface.

The measurement of force–distance curves through AFM is obtained by recording the AFM cantilever deflection as a function of its vertical displacement when the tip is pressed against the surface of the sample (loading curve), and then removing it (unloading curve) at a given rate. The indentation depth can be derived from the experimental data, and corresponds to the difference between the probe vertical movement and its deflection.

* Corresponding author. Tel.: +39 0223993249; fax: +39 0270638173.
E-mail address: raffaella.suriano@polimi.it (R. Suriano).

The indentation measurements can be related to the elastic modulus of the sample. To obtain the Young's modulus, it is necessary to apply a mathematical model describing the contact between the tip and the surface. Several theories describe the elastic deformation of the sample [33,36–39], and the differences in the mathematical equations mostly depend on the role played by the adhesion in the system under investigation. The classical Hertz model does not consider the adhesive contribution, and it is therefore applicable only when the adhesion interaction is negligible compared to the loading force, as in the case of stiff materials in dry environment, or when the analysis is conducted in an aqueous environment [33,37,38]. Other models were derived from the Hertz model for tests conducted in air, in particular the Johnson–Kendall–Roberts (JKR) and the Derjaguin–Müller–Toporov (DMT) that both consider the adhesive contribution in the outside (JKR) or inside (DMT) of the contact area [33,37,38,40]. In addition to these analytical models, several instrumental factors such as tip shape, spring constant and z-piezoelectric scanner movement can largely influence the quantification of the elastic moduli [41–44].

In this paper, an adaptable method to measure force–distance curves in air by means of an AFM instrument is presented for the determination of the Young's modulus for a series of highly diversified polymeric materials, like hydrogels, sol–gel hybrids, thermoplastics, and elastomers. Actually, no careful investigation on the selection of the cantilever spring constant and geometrical features of AFM probes to achieve an optimal indentation range of diverse samples was presented so far in the scientific literature. In order to take into account the different stiffness and adhesion phenomena, a thorough evaluation and comparison of various mathematical models is however necessary and still to be accomplished. In the present study, several mathematical theories such as Hertz, Sneddon, DMT, JKR and Pietrement–Troyon (PT) models are applied critically discussing their application limits and threshold. A proper probe selection in terms of spring constant and tip shape is also discussed for all the samples under investigation. In addition, a hydrophobic surface functionalization of the probe is developed and examined in order to minimize adhesion phenomena on soft samples. More specifically, the hydrophobic treatment of the tips was introduced to decrease capillary forces which cause high tip-surface adhesion. This surface modification allowed the challenging evaluation of Young's modulus of very soft and aqueous samples by AFM indentation in air. The results derived from the AFM nanoindentation tests were compared with literature data or with independent determinations derived from dynamic mechanical measurements in order to evaluate their reliability. We believe that this study will therefore provide helpful and general guidelines for the AFM nanoindentation measurements of elastic moduli in air for a wide range of polymeric materials with very diverse characteristics that encompasses very soft hydrogels and stiff hybrid organic–inorganic coatings.

2. Theoretical background

Different approaches were employed to determine the elastic modulus from indentation experiments. The classical theory for a spherical indenter of radius R on a planar surface was first developed by Hertz in 1882 [45]. Using the Hertz model, the relationship between the applied force, F and the elastic indentation depth δ is represented by the following equation:

$$F = E_{tot} R^{1/2} \delta^{3/2} \tag{1}$$

where E_{tot} is the total modulus, which is defined as follows:

$$\frac{1}{E_{tot}} = \frac{3}{4}\left(\frac{\left(1-\nu_s^2\right)}{E_s} + \frac{\left(1-\nu_t^2\right)}{E_t}\right) \tag{2}$$

being E_s, ν_s and E_t, ν_t the Young's moduli and the Poisson's ratios for the sample and the tip, respectively [46]. By neglecting the deformation of the tip, which can be considered infinitely stiff when compared to the sample, the Eq. (2) is simplified to:

$$\frac{1}{E_{tot}} = \frac{3}{4}\left(\frac{\left(1-\nu_s^2\right)}{E_s}\right). \tag{3}$$

Starting from the classical Hertz theory, another equation suitable for a conical indenter was proposed by Sneddon [47] and according to this model, F is related to indentation by:

$$F = \frac{2}{\pi}\tan\alpha \frac{E_s}{\left(1-\nu_s^2\right)}\delta^2 \tag{4}$$

where α is the half-opening angle of an AFM conical tip.

Using the Hertz and Sneddon models, adhesion phenomena are assumed to be negligible and do not affect the sample deformation. In case of interactions between tips and samples strongly influenced by adhesion, both the Derjaguin–Müller–Toporov (DMT) [48] and the Johnson–Kendall–Roberts (JKR) models [49] can be employed for spherical tips. The DMT model is suitable for samples with small adhesion force, F_{ad} and is represented by the following equation:

$$F + F_{ad} = \frac{4E_s}{3\left(1-\nu_s^2\right)} R^{1/2}\delta^{3/2} \tag{5}$$

where F_{ad} can be also defined as the pull-off force, at which the tip and the sample separate when being pulled apart. The DMT theory also predicts that the contact radius a between the tip and the sample and the indentation depth δ are given by:

$$\delta = \frac{a^2}{R} \tag{6}$$

$$a = \left[\frac{R}{E_{tot}}\left(F + F_{ad}\right)\right]^{1/3}. \tag{7}$$

When large adhesion phenomena are observed, the more complex JKR model can be used and expressed by the following equations:

$$\delta = \frac{a^2}{R} - \frac{4}{3}\sqrt{\frac{aF_{ad}}{RE_{tot}}} \tag{8}$$

$$a = \left[\frac{R}{E_{tot}}\left(\sqrt{F_{ad}} + \sqrt{F + F_{ad}}\right)^2\right]^{1/3} \tag{9}$$

In all AFM measurements the extent of indentation depends on the contact radius, tip radius and adhesion force eventually present [33]. The applied force is directly related to the cantilever deflection through the Hooke's law:

$$F = k\left(d - d_1\right) \tag{10}$$

where k is the spring contact of the cantilever and d_1 is the zero-deflection point of the cantilever.

The AFM does not provide direct measurements of force and indentation depth. The sample indentation δ is obtained by the difference between the probe vertical displacement $\Delta z = (z - z_0)$, and the AFM cantilever deflection $\Delta d = (d - d_0)$, where z_0 and d_0 are, respectively, the zero indentation position of the z-piezo and of the cantilever, corresponding to the contact point:

$$\delta = (z - z_0) - (d - d_0). \tag{11}$$

The point of zero applied force (z_1, d_1) and the zero indentation point (z_0, d_0) are coincident only in Hertzian mechanics. By

combining the Eqs. (1) or (4) with (10) and (11), the Hertz and Sneddon models can be thus expressed as follows, respectively:

$$z = z_0 + (d - d_0) + \left(k(d - d_0) \frac{3\left(1 - \nu_s^2\right)}{4E_s R^{0.5}} \right)^{2/3} \tag{12}$$

$$z = z_0 + (d - d_0) + \left(k(d - d_0) \frac{\pi\left(1 - \nu_s^2\right)}{2E_s \tan\alpha} \right)^{1/2}. \tag{13}$$

A relationship between δ and F can be obtained using the Pietrement–Troyon (PT) model [50], which describes adhesion dominated contact mechanics and includes the DMT and JKR models as two limiting cases by means of a generalized transition equation. According to PT model, the DMT equation becomes:

$$z = z_0 + (d - d_0) + \frac{a_0^2}{R} \left(\sqrt{\frac{1 + k(d - d_1)}{F_{ad}}} \right)^{4/3} \tag{14}$$

where a_0 is the contact radius when $F = 0$. Applying the Eq. (14) to the raw AFM curves, the value of a_0 is eventually determined and the modulus of the sample E_s can be calculated by:

$$E_s = \left(1 - \nu_s^2\right) \frac{3F_{ad}R}{4a_0^3} \tag{15}$$

obtained by setting $F = 0$ in Eq. (7), substituting the definition of E_{tot} given by Eq. (3) and solving for E_s.

The PT model gives the following expression for the JKR theory:

$$z = z_0 + (d - d_0) + \frac{a_0^2}{R} \left(\left(\frac{1 + \sqrt{1 + k(d - d_1)/F_{ad}}}{2} \right)^{4/3} - \frac{2}{3} \left(\frac{1 + \sqrt{1 + k(d - d_1)/F_{ad}}}{2} \right)^{1/3} \right) \tag{16}$$

and the modulus E_s is obtained by setting $F = 0$ in Eq. (9), substituting the definition of δ and of E_{tot} given by Eq. (8) and by Eq. (3), respectively, and solving for E_s, as follows:

$$E_s = \left(1 - \nu_s^2\right) \frac{3F_{ad}R}{a_0^3}. \tag{17}$$

3. Experimental part

3.1. Materials

All the reagents were used without any purification. Ethanol, hydrogen peroxide (30% w/w), H_2SO_4 (95–97%), 1*H*,1*H*,2*H*,2*H* perfluorodecyltriethoxysilane (PFDTES, 97%), tetraethylorthosilicate (TEOS), hyaluronic acid solution salt from streptococcus equi-bacterial glycosaminoglycan polysaccharide, divinyl sulfone, and HPLC pure water were all purchased from Sigma-Aldrich. Dimethyldichlorosilane (DMDCS, 99.0%) and γ-propyl-isocyanate triethoxysilane were purchased from Fluka. Silicon wafers were purchased from SILTRONIC AG, and all the Esco® microscope slides are from Erie Scientific LLC. Poly(methyl methacrylate) (PMMA) samples (Perspex XT, bulk samples from injection molding) were supplied from Lucite. $Fs_{36}S_{62}$ is an experimental organic–inorganic hybrid coating synthesized by sol–gel chemistry and applied on cleaned glass substrates as described previously [51]. In brief, this particular hybrid material consists of 36 wt.% of a fluorocarbon resin (Lumiflon LF-910 from Asahi Glass, Japan), which is a chlorotrifluoroethylene–vinylether copolymer used as base fluoropolymer, 1.6 wt.% of SiO_2 wt.% derived from the functionalization of fluoropolymer resin with γ-propyl-isocyanate triethoxysilane and 62.4 wt.% of SiO_2 derived from TEOS [51]. Polydimethylsiloxane (PDMS) samples (Sylgard 184, Dow Corning Corporation) with a thickness of 1 mm were obtained using a two-component heat curing system, composed of a pre-polymer and a cross-linker (curing agent). In this study, the pre-polymer was mixed with the curing agent in the weight ratio of 10/1. Hyaluronic acid hydrogels (HA) were diluted in NaOH 0.5 M solutions up to 3% w/v solid. Divinyl sulfone (DVS) was added as a crosslinker in separate experiments (5/1 molar with respect to HA primary hydroxyls), and crosslinked at 40 °C for 24 h before testing. Samples with various thickness (0.4–2 mm) were obtained by casting [52].

3.2. AFM measurements and data fitting

Every force–distance curve was obtained in air by means of an NSCRIPTOR™ atomic force microscope (NanoInk, Inc., Skokie, IL). The NSCRIPTOR™ instrument, designed and developed for Dip-Pen Nanolithography applications, is provided with a closed-loop correction, which consists in a piezo scanner fitted with a secondary monitoring system that has its own feedback loop. This allows the closed-loop scanner to perform with a high degree of linearity, as also certified in the NanoInk datasheet (Supplementary materials). In addition, to correct time-independent non-linearity of the scanner, before any experimental round, a linearization procedure available in the SPMCockpit was carried out, determining the optimum linear range of the *x*–*y* feedback sensors (*x*–*y* area in which the scanner is currently linear). All the probes were purchased from AppNano (Santa Clara, CA, USA). Every curve was performed with a tip rate of 0.05 Hz and evaluated using the Cockpit® software. Fitting of the raw AFM curves was carried out by means of OriginPro 8.5 software and the quality of the fitting was evaluated in terms of coefficient of determination R^2 (the maximum number of iterations was set to 400 for each fitting). For the fitting, all the datasets were firstly restricted so that the maximum penetration depth of the tip into the sample was acceptable for the mathematical models considered. In particular, for the Hertz, DMT and JKR model, this implies that the maximum penetration depth should be comparable to the tip radius. The datasets were then limited to the beginning of the experimental range in order to consider not only the elastic part of deformations but also a range of indentations lower than 0.1% of sample thickness. This prevented the stiffness of substrates from affecting modulus measurements of samples. The datasets were lastly selected from a statistical point of view. The adjusted R^2 coefficient was compared for different datasets in order to select a dataset with an adjusted R^2 value higher than 0.99. This coefficient was considered as a reliable measure of the goodness of interpolation, and is defined by the following equation:

$$\text{adjusted } R^2 = 1 - \frac{\sum_{i=1}^{n} (y_i - \hat{y})^2 / (n - k)}{\sum_{i=1}^{n} (y_i - \bar{y})^2 / (n - 1)} \tag{18}$$

where y_i and $\hat{y}$ are the original measured data values and modeled values, respectively, $\bar{y}$ is the mean of the observed data, n is the number of dataset points and k is the number of parameters calculated by the interpolation. As shown by the Eq. (18), the adjusted R^2 value allows for the number of dataset points that corresponds to the size of the considered range and it is higher by increasing the number of dataset points. This method, therefore, avoided a very small portion of curves being selected.

3.2.1. Probes calibration

All probes were calibrated by applying a load on a substrate (a piranha-cleaned Si surface), much stiffer than polymers so that no indentation occurred. The calibration of probes is needed to calculate the probe sensitivity, a parameter that converts the cantilever

deflection signal from mV to nm. Every calibration was carried out loading the reference surface with a maximal cantilever deflection of 400–500 nm. The sensitivity is then obtained by calculating the slope of the contact linear part of the force–distance curves gained.

3.2.2. Characterization of PMMA and $Fs_{36}S_{62}$ coatings

Every sample surface was blown with a dry nitrogen flux to remove most of the impurities from the surfaces. PMMA surfaces and hybrid inorganic–organic coatings were analyzed with standard ACT mounted probes (AppNano, Santa Clara, CA, USA), whose spring constants were calculated by the Sader method [53], resulting in a value of 36 N/m for PMMA and 63.3 N/m for $Fs_{36}S_{62}$. For PMMA samples, force curves were carried out at three different rates (0.05, 1 and 10 Hz), using the same tip rate for loading and unloading curves. In order to control and minimize the adhesive forces due to the formation of a water meniscus between the tip and the sample surface, AFM indentation tests were carried out with a relative humidity ≤15%. Just after the tip approach in contact mode, the probe was raised in order to avoid any interaction between the probe and the surface that could affect the indentation. To prevent that an indentation experiment could affect the following one, the position of probes was changed after every applied load, including the approach procedures. All the measurements were carried out in at least 20 different areas of the samples, and the results were averaged.

3.2.3. Characterization of PDMS elastomers

Silicone rubber samples were analyzed using two spherical probes, HYDRA 6R100NG (k = 0.757 N/m) and HYDRA 6R200NG (k = 0.035 N/m) probes with a colloidal SiO_2 tip (tip radius = 2.5–4.5 μm) in a controlled atmosphere with a relative humidity ≤15%. HYDRA 6R200NG probes were silanized in air with PFDTES at 100 °C overnight to reduce the strong adhesive interactions observed between very flexible probes and compliant PDMS samples. To obtain the force–distance curves on these samples, the same procedure used to indent the stiffer samples was applied.

3.2.4. Characterization of hyaluronic acid hydrogels

All the samples were supported over a glass microscope slide. Since the swelled hydrogel must remain hydrated, all the samples were indented just after the hydration process, keeping a constant relative humidity of 50%. Colloidal probes (series HYDRA 6R200NG, k = 0.035 N/m) were used to analyze the hydrogel samples and silanized in air with PFDTES at 100 °C overnight to make it hydrophobic. After any AFM indentation, the probe was retracted from the surface and moved off to avoid any interaction with the sample or the water layer on the hydrogel surface before any subsequent indentation.

3.3. Dynamic–mechanical measurements

Dynamic mechanical analysis (DMA) was performed with a DMA/SDTA861e Mettler Toledo dynamic mechanical analyzer. PMMA specimens with a thickness of 2 mm, a width of 14 mm and a length of 75 mm were mounted in a three-point bending accessory and analyzed at 25 °C with displacement-controlled scans from 1 μm to 400 μm and oscillation frequency of 0.05 Hz and 1 Hz. As for PDMS samples, 1.5 mm thick, round specimens with a diameter of 6.7 mm were tested in shear mode at 25 °C in the linear viscoelastic range, with dynamic shear displacement-controlled scans from 0.1 μm to 100 μm and oscillation frequency of 0.05 Hz. The HA hydrogel samples were analyzed by a stress-controlled rotational rheometer Rheometrics Dynamic Stress Rheometer 200. Frequency sweep tests were performed in a frequency range of 0.01–1 Hz, with 25 mm parallel plates at 37 °C, after having checked the linear viscoelastic range in separate experiments.

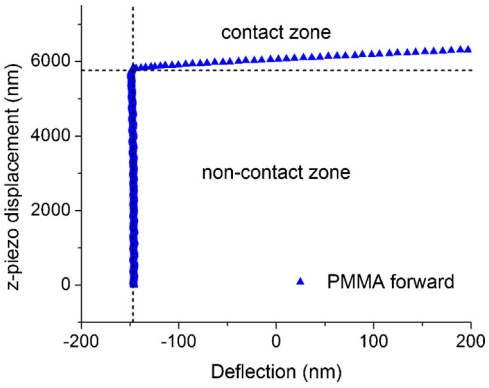

Fig. 1. z-Piezo displacement vs. forward deflection curve measured by AFM on a PMMA surface (the initial values of cantilever deflection are negative because the probe was lifted up before indentation test to prevent any possible interaction with the surface).

4. Results and discussion

The elastic modulus was investigated for a variety of different materials by means of AFM nanoscale indentation tests. Fig. 1 shows a typical forward raw curve obtained directly by AFM on a surface of PMMA.

Notwithstanding a positive piezo displacement z in the starting part of the loading curve, no variation in cantilever deflection is measured by AFM, because the tip is not still in contact with the surface of sample when the piezoelectric system begins to move the probe toward the sample (non-contact region). When the tip reaches the surface, an abrupt change in the deflection of cantilever is then observed (contact part). By interpolating the contact part of raw curves in the form of vertical piezo displacement z as a function of cantilever deflection d, it is possible to determine the zero indentation point of the z-piezo z_0 and the elastic modulus of samples E_s through the estimation of δ according to the Hertz (Eq. (12)), Sneddon (Eq. (13)), DMT (Eq. (14)) and JKR (Eq. (16)) equations. When adhesive interactions are observed, the DMT and JKR models are more suitable than two others, as discussed in Section 2.

In our experiments, reliable force vs. displacement curves were obtained on PMMA surfaces using a probe with a pyramidal tip and a stiff cantilever (spring constant k = 36 N/m) (Fig. 2a). Fig. 2a shows that the reverse (unloading) curve does not overlap with the forward (loading) curve. This result is due to PMMA plastic deformation during the loading phase and shows that the sample cannot recover completely the deformation at the end of the unloading phase [54]. As indicated by the presence of a plastic deformation in the loading phase (Fig. 2a), the unloading curves also appeared to be more suitable than the loading ones to determine elastic modulus from AFM indentation tests due to the absence of plastic effects, as also confirmed by previous works [41,55].

In order to calculate the elastic modulus, the zero deflection d_0 was determined as the first point in the non-contact part of force curves and a Poisson's ratio ν_s of 0.35 was assumed for PMMA [56]. Considering that adhesive forces are negligible for PMMA samples (as visible in Fig. 2a), interpolation of displacement vs. deflection curves of PMMA according to the Hertz and Sneddon models was performed by employing the Eqs. (12) and (13), respectively. The determination of two unknown parameters was thus allowed by using the Eqs. (12) and (13): the zero indentation position of the piezo z_0 and the Young's modulus E_s. These results made also possible the calculation of the indentation δ according to the Eq. (11) (Fig. 2b). A maximum indentation δ_{max} of approximately 150 nm

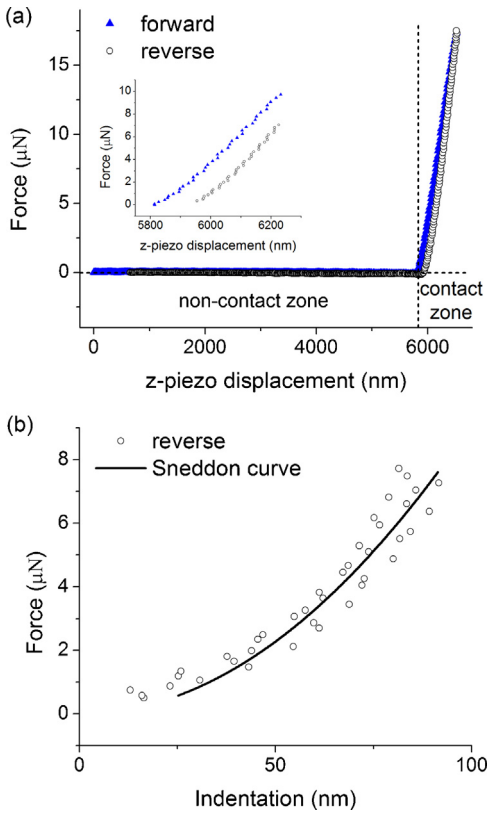

Fig. 2. (a) Force vs. *z*-piezo displacement curve in the complete *x*-range, (inset) in the range where the curve was interpolated and (b) force vs. indentation curve obtained from unloading phase with superimposed Sneddon model curve in the dataset selected for the fitting performed by employing the Eqs. (4) and (13) for PMMA samples.

and 90 nm was found, respectively, considering the forward and reverse curves (Table 1). Initially, for the determination of E_s, a tip radius R of 6 nm was used for the Hertz model (Eq. (12)) and a half-opening angle α of 18° for the Sneddon model (Eq. (13)), as suggested by the nominal specifications provided by the AFM probe manufacturer and checked by electron microscopy (SEM). However, the tips were checked by SEM after the AFM indentations and a variation in features and dimensions was found out. The tip radius was changed from 6 nm to 340 nm and the half-opening angle from 16° to 24° (Fig. S2). The elastic modulus recalculated with the Sneddon model and with the half-opening angle after measurements was found more consistent to the reference value. In addition, the values of maximum indentation suggest that the tip penetrates considerably and deeply into the sample during indentation, behaving like a sharp indenter (Table 1). This behavior of the tip can be approximated by the Sneddon model (conical indenter) better than the Hertz model. Consequently, it is clear the fitting of reverse curves with the Sneddon model is the most appropriate method to assess nanoscale mechanical behavior of PMMA.

With the aim of considering viscoelastic effects on AFM indentations of PMMA, different tip rates were employed to perform force curves on this sample [57–60]. As shown in the Supplementary materials (Table S1 and Fig. S1), the values of maximum indentations obtained at 1 and 10 Hz were lower than at 0.05 Hz. Furthermore, the corresponding elastic modulus obtained from unloading curves with the Sneddon model are found to be higher by increasing the tip rate. Stiffening of PMMA samples is mainly due to the distinctive time-dependent behavior of polymers [61], as also confirmed by measurements performed with well-established techniques such as DMA (Table S1). It is supposed that viscoelasticity of crosslinked polymers such as those analyzed below is less evident.

By employing softer cantilevers with a spring constant of 0.035 and 0.757 N/m, no corresponding indentations were found on PMMA (data not shown). This indicates that soft cantilevers cannot apply forces high enough to deform thermoplastic surfaces, and are too compliant compared to the sample. In contrast, cantilevers with a spring constant of nearly 30–40 N/m are suitable to perform nanoscale indentation tests on thermoplastic polymers such as PMMA. Force–distance curves were also measured on PMMA using spherical tips with a tip radius of 2500 nm attached to stiff cantilevers but the maximum value of elastic indentation was quite low (~30 nm), leading to a poor quality of modulus prediction from force curves (data not shown).

With regard to $Fs_{36}S_{62}$ hybrid coatings, Fig. 3a shows that forward and reverse curves obtained with a pyramidal tip and a stiff cantilever (k = 63.3 N/m) overlapped very well each others, suggesting a pure elastic behavior of this highly crosslinked material. In addition, likely due to the low surface tension fluoropolymer resin present in $Fs_{36}S_{62}$ coatings, no relevant adhesive interactions were observed between silicon tips and such surfaces (Fig. 3a).

Considering the range of indentations obtained for $Fs_{36}S_{62}$ surfaces (Table 1), the tip can be properly approximated to a sharp pyramidal indenter and therefore the prediction of elastic modulus was performed also in this case by employing the Sneddon model and a half-opening angle of 24.2°, checked by SEM after measurement session. Data present in literature for organic-inorganic hybrid coatings are in the range of 4–8 GPa [62,63], and appear to be rather lower than those shown in the present study. However, it should be noticed that $Fs_{36}S_{62}$ hybrid coatings have a much higher fraction of inorganic components, thus resulting in higher values of E_s. Cantilevers with a spring constant of about 35 N/m and pyramidal tips were also used to indent these hybrid surfaces. However, due to very low penetration depths obtained, this type of cantilevers appeared inappropriate for AFM indentation tests on hybrid coatings (data not shown).

The effect of cantilever spring constants on indentations measurements was also investigated for softer samples. Silicone samples are sufficiently soft to be indented with spherical probes which are more conveniently modeled through the various equations. The force vs. displacement curve obtained on a PDMS surface using a spherical tip and a cantilever with k = 0.757 N/m is shown in Fig. 4a. As a comparison, AFM indentation tests were also carried out on PDMS employing a cantilever with a lower constant spring (k = 0.035 N/m) (Fig. 5a). In the latter case, however, a hydrophobic silanization of the tip with PFDTES was needed to reduce strong adhesion interactions between SiO_2 spherical tip and PDMS surface.

Table 1
Poisson's ratio, average maximum indentation, elastic modulus obtained using the Sneddon models and reference Young's modulus values for PMMA and $Fs_{36}S_{62}$ samples.

		Poisson's ratio ν_s	Indentation δ (nm)	E_s (Sneddon) (GPa)	Reference E value (GPa)
PMMA	Forward	0.35	153 ± 12	1.7 ± 0.3	3.2 ± 0.6*
	Reverse		89 ± 3	2.8 ± 0.6	
$Fs_{36}S_{62}$	Forward	0.2	47 ± 12	30.4 ± 7.5	n.a.
	Reverse		54 ± 10	19.6 ± 4.8	

* Value measured by dynamic mechanical analysis at 0.05 Hz.

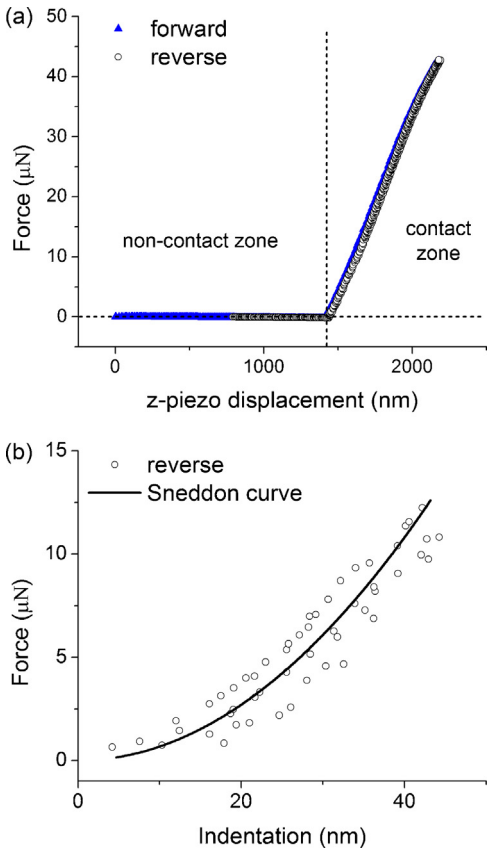

Fig. 3. (a) Force vs. *z*-piezo displacement curve and (b) force vs. elastic indentation curve obtained from reverse phase with superimposed Sneddon model curve in the dataset selected for the fitting performed by employing the Eqs. (1) and (12) for $Fs_{36}S_{62}$ surfaces.

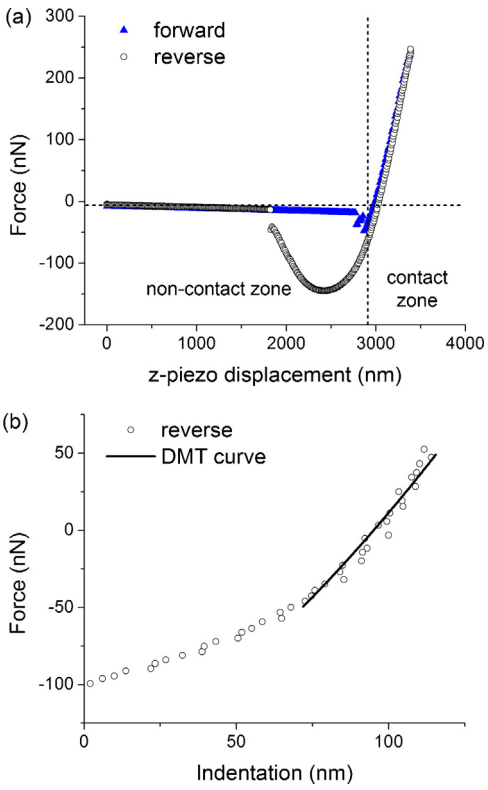

Fig. 4. (a) Force vs. *z*-piezo displacement curve using a probe with a spring constant of 0.757 N/m and (b) force vs. indentation curve obtained from reverse phase with superimposed DMT model curve in the dataset selected for the fitting performed by employing the Eqs. (5) and (14) for a PDMS surface.

In fact, the contact part of curves is significantly reduced or even not present, if these adhesion-dominated interactions are predominant as observed without the hydrophobic treatment of tips (Fig. S3). Pristine silicon-based AFM tips are strongly attracted by PDMS surfaces and in case of very soft cantilever, the *z*-piezo is engaged in the non-contact part of curves with the adhesive phenomena for the majority of its displacement. As suggested by the nearly complete overlapping of the forward and reverse curves in Figs. 4a and 5a, this elastomeric sample exhibits an elastic behavior. Strong adhesion forces are however evident especially in unloading phase. Van der Waals attractive forces, which are smaller than adhesive forces in the unloading phase, were also noticed in loading curves. This finding suggests that AFM raw data for PDMS sample have to be analyzed according the DMT (Eq. (14)) and JKR (Eq. (16)) models.

According to the literature, the JKR approach is more valid for compliant materials and cases with high interfacial energies [49], while the DMT theory is known to be applicable to stiffer samples and low interfacial energies [48]. Accordingly, the DMT model was preferentially applied to analyze the force displacement curves on PDMS surfaces. However, the JKR model was tentatively employed to interpolate the unloading curves because attractive interactions appeared to be considerably high relative to the contact forces in the reverse curves. For the interpolation of curves applying the DMT and JKR models, datasets were selected as that the point where $F = 0$ was included and the value of R^2 was as high as possible, as discussed in Section 3.2. Table 2 shows that the values of E_s calculated using the JKR model are systematically higher than those measured by macroscopic dynamic mechanical analysis. This suggests that the JKR model tends to overestimate the elastic modulus of PDMS and therefore provides a less reliable prediction of elastic modulus for rubbery samples such as PDMS.

Considering the force curves measured using a cantilever with $k = 0.757$ N/m, the DMT model gives a value of elastic modulus for PDMS in very good agreement with that obtained by macroscopic mechanical measurements. By employing a probe with a lower spring constant ($k = 0.035$ N/m), a low elastic indentation was reached and the estimate of elastic modulus according to the DMT model was slightly higher when compared to the reference value (Fig. 5b and Table 2). These results suggest that the DMT model is more appropriate than the JKR model to analyze samples with modulus similar to that of PDMS by means of AFM indentation tests. In addition, a spring constant of approximately 0.757 N/m appears to be suitable in this case because a good value of maximum indentation can be obtained (Fig. 4b) and a moderate adhesion force relative to the max applied force can be observed.

AFM indentation experiments were also performed in air on surfaces of hyaluronic acid hydrogels crosslinked with divinyl sulfone (for brevity, these hydrogels will be referred to as HA:DVS from here on). These samples required a very flexible probe to get indented properly. Hydrogels are very soft and wet, therefore the adhesive forces are predominant in this case. Initially, pristine spherical tips were employed. However a sharp adhesion attraction of the tips toward the water layer above the hydrogel surface was noted, due to the high water content in HA:DVS hydrogels. Due to this strong adhesion phenomenon, the tip was not allowed to move to any directions, making the loading and unloading phases unfeasible. A hydrophobic coating was therefore deposited on the probes with two different silanes in order to analyze these samples. DMDCS was firstly used to silanized spherical tips, but it still led to several approach and adhesion issues due to the meniscus effect. The probes were finally silanized with PFDTES, resulting in an effective

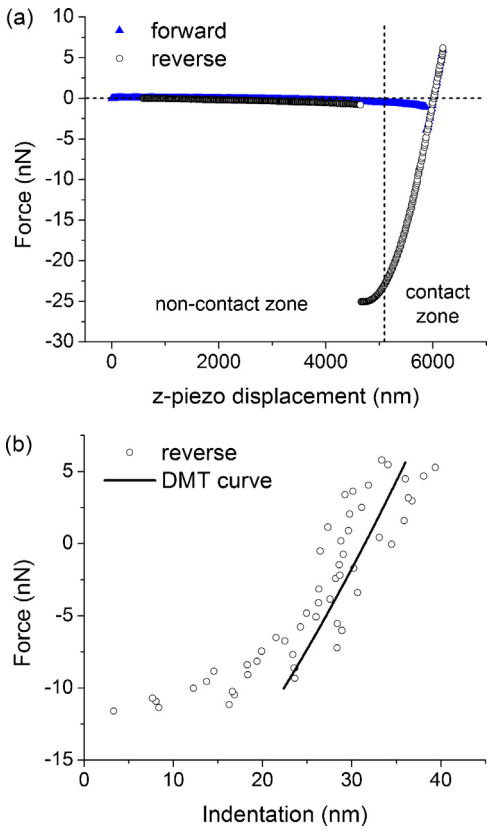

Fig. 5. (a) Force vs. *z*-piezo displacement curve using a probe with a spring constant of 0.035 N/m and (b) force vs. indentation curve obtained from reverse phase with superimposed DMT model curve in the dataset selected for the fitting performed by employing the Eqs. (5) and (14) for a PDMS surface.

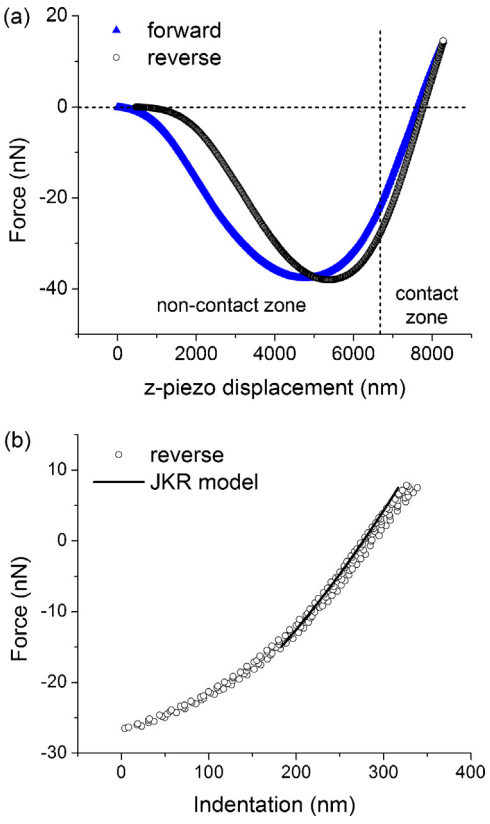

Fig. 6. (a) Force vs. *z*-piezo displacement curve measured using a PFDTES silanized probe with a spring constant of 0.035 N/m and (b) force vs. indentation curve obtained from reverse phase in the dataset selected for the fitting performed by employing the Eq. (16) for a HA:DVS 1:5 hydrogel sample.

control of adhesion phenomena. Accordingly, probes silanized with PFDTES were definitely chosen to perform all the tests on hydrogel samples.

Fig. 6 shows the force vs. displacement and force vs. indentation curves obtained on a HA:DVS hydrogel samples using a cantilever with a spring constant of 0.035 N/m. Stiffer cantilevers did not provide any appreciable indentation on HA:DVS hydrogels. As shown in Fig. 6a, the deflection and force due to the adhesion are much higher than the applied force and this affects both the loading and unloading curves [64]. In case of PDMS, the adhesion caused a sudden change in the deflection value, while the curves obtained on the hydrogel are broader and the change induced by adhesion is smoother. As opposed to PDMS, the loading and unloading curves of HA:DVS are not overlapped, suggesting the presence of dissipation phenomena due to the viscoelastic nature of the hydrogel and high water content of these crosslinked hydrogels. These phenomena could also explain the difference in the values of E_s obtained from forward and reverse curves (Table 2). Interpolation of the forward curves according to the DMT and JKR models provide a value of Young's modulus lower than those obtained for reverse curves. This difference was observed both applying the DMT and JKR models, which provide a comparable estimate of modulus. These values of modulus were compared with values derived from rheological measurements performed in a previous paper [52] on a hydrogel swelled in water, taking into account that the two analyses were performed at different temperature, i.e. $T_{AFM} = 25\,^{\circ}C$ and $T_{RH} = 37\,^{\circ}C$ The values of E_s obtained from AFM indentations tests are higher than the elastic modulus by rheological measurements. This difference may be partially attributed to some source of uncertainty in AFM-based property measurements, such as the actual cantilever spring constant and the AFM tip shape [39,41,65]. However it is likely that for these samples a major source of systematic error is the partial loss of water during the indentation experiments carried out in air that contributed to make the hydrogels stiffer than those completely swelled.

Table 2
Spring constant, Poisson's ratio, averaged maximum indentation, adhesion force, Young's modulus obtained using both DMT and JKR models and reference Young's modulus values for PDMS and HA:DVS 1:5 hydrogel samples.

		Spring constant k (N/m)	Poisson's ratio ν_s	Indentation δ (nm)	Adhesion force F_{ad} (nN)	E_s (DMT) (kPa)	E_s (JKR) (kPa)	Reference E value (kPa)
PDMS	Fwd	0.757	0.5	155 ± 40	144.5 ± 2.2	1302 ± 118	2037 ± 637	1240 ± 46*
	Rev			112 ± 16		1651 ± 908		
	Fwd	0.035	0.5	36 ± 2	25.1 ± 0.01	1509 ± 182	1709 ± 69	
	Rev			34 ± 5		1582 ± 63		
HA:DVS	Fwd	0.035	0.5	638 ± 55	38.5 ± 0.4	20.2 ± 3.0	22.0 ± 3.2	4.4 ± 0.4 [52]
	Rev			335 ± 66		69.6 ± 20.3	75.6 ± 22.3	

* Value measured by dynamic mechanical analysis.

5. Conclusive remarks

This study presents a critical review of existing theoretical models and the development of an adaptable method for the measurements of Young's modulus for a variety of polymeric and hybrid materials in air by means of an AFM instrument. Elastic moduli ranging from 10^1 kPa to 10^1 GPa were estimated and are in good agreement with rheological and mechanical measurements and with literature data, even allowing for the source of uncertainty in calibration of cantilever stiffness and tip probe geometry. This work also shows how the spring constant of cantilevers in AFM indentation should be chosen mainly taking account of the intrinsic elastic properties of the sample. A careful selection of cantilever spring constant and geometrical features is indeed important to achieve an optimal indentation range of the sample. More precisely, a cantilever with a spring constant of 30–40 N/m and 50–60 N/m is recommended for samples relatively stiff up to about 3 GPa and 10–20 GPa, respectively. In both cases a pyramidal tip is found to be suitable to perform AFM indentations. In case of soft samples with an elastic modulus of a few thousands of kPa, a max indentation depth of 100 nm, which is appropriate and reliable, was measured using cantilevers with a spring constant of 0.5–1 N/m and a spherical tip. For very soft materials with 1–100 kPa of modulus, the spring constant of cantilevers should be approximately 0.035 N/m and a spherical tip is suggested. The experiments were typically carried out in air, allowing a faster and easier sample handling and laser setting on the cantilever when compared to tests carried out in a liquid environment. Significant adhesion phenomena were observed where flexible cantilevers were used, but they were effectively controlled carrying out an easy preliminary hydrophobic treatment of tips. The main limitation of measurements performed in air is probably that of hydrogel samples, due to a partial evaporation of the water during the test. In these specific cases AFM nanoindentation tests can still be used for an approximated estimate of elastic moduli of very soft samples.

Acknowledgments

The research was funded by Cariplo Foundation, Milano, Italy, grant number 2010/0365, project "3D Micro structuring and Functionalization of Polymeric Materials for Scaffolds in Regenerative Medicine". Special thank to Gigliola Clerici for rheological measurements and technical support and to Dario Picenoni for SEM analyses.

Appendix A. Supplementary data

Supplementary data associated with this article can be found, in the online version.

References

[1] M. Lekka, K. Pogoda, J. Gostek, O. Klymenko, S. Prauzner-Bechcicki, J. Wiltowska-Zuber, J. Jaczewska, J. Lekki, Z. Stachura, Cancer cell recognition—mechanical phenotype, Micron 43 (2012) 1259–1266.
[2] N. Gavara, R.S. Chadwick, Determination of the elastic moduli of thin samples and adherent cells using conical atomic force microscope tips, Nat. Nanotechnol. 7 (2012) 733–736.
[3] P. Schaer-Zammaretti, J. Ubbink, Imaging of lactic acid bacteria with AFM—elasticity and adhesion maps and their relationship to biological and structural data, Ultramicroscopy 97 (2003) 199–208.
[4] B. Bhushan, Nanotribological and nanomechanical properties of skin with and without cream treatment using atomic force microscopy and nanoindentation, J. Colloid Interface Sci. 367 (2012) 1–33.
[5] M. Mustata, K. Ritchie, H.A. McNally, Neuronal elasticity as measured by atomic force microscopy, J. Neurosci. Methods 186 (2010) 35–41.
[6] M.A. Beckmann, S. Venkataraman, M.J. Doktycz, J.P. Nataro, C.J. Sullivan, J.L. Morrell-Falvey, D.P. Allison, Measuring cell surface elasticity on enteroaggregative *Escherichia coli* wild type and dispersin mutant by AFM, Ultramicroscopy 106 (2006) 695–702.
[7] P. Tracqui, A. Broisat, J. Toczek, N. Mesnier, J. Ohayon, L. Riou, Mapping elasticity moduli of atherosclerotic plaque in situ via atomic force microscopy, J. Struct. Biol. 174 (2011) 115–123.
[8] D. Passeri, A. Bettucci, A. Biagioni, M. Rossi, A. Alippi, E. Tamburri, M. Lucci, I. Davoli, S. Berezina, Indentation modulus and hardness of viscoelastic thin films by atomic force microscopy: a case study, Ultramicroscopy 109 (2009) 1417–1427.
[9] A. Tiwari, Nanomechanical analysis of hybrid silicones and hybrid epoxy coatings—a brief review, Adv. Chem. Eng. Sci. 2 (2012) 34–44.
[10] J. Alvarado-Rivera, J. Muñoz-Saldaña, R. Ramírez-Bon, Nanoindentation testing of SiO_2-PMMA hybrid films on acrylic substrates with variable coupling agent content, J. Sol–Gel Sci. Technol. 54 (2010) 312–318.
[11] J. Ballarre, E. Jimenez-Pique, M. Anglada, S.A. Pellice, A.L. Cavalieri, Mechanical characterization of nano-reinforced silica based sol–gel hybrid coatings on AISI 316L stainless steel using nanoindentation techniques, Surf. Coat. Technol. 203 (2009) 3325–3331.
[12] A.J. Atanacio, B.A. Latella, C.J. Barbé, M.V. Swain, Mechanical properties and adhesion characteristics of hybrid sol–gel thin films, Surf. Coat. Technol. 192 (2005) 354–364.
[13] J. Domke, M. Radmacher, Measuring the elastic properties of thin polymer films with the atomic force microscope, Langmuir 14 (1998) 3320–3325.
[14] H. Kaczmarek, P. Gałka, Nano-mechanical properties of modified poly(methyl methacrylate) films studied by atomic force microscopy, Tribol. Lett. 41 (2011) 541–554.
[15] A. Pakzad, J. Simonsen, R.S. Yassar, Elastic properties of thin poly(vinyl alcohol)–cellulose nanocrystal membranes, Nanotechnology 23 (2012) 085706.
[16] M. Alderighi, V. Ierardi, M. Allegrini, F. Fuso, R. Solaro, An atomic force microscopy tip model for investigating the mechanical properties of materials at the nanoscale, J. Nanosci. Nanotechnol. 8 (2008) 2479–2482.
[17] M. Radmacher, M. Fritz, P.K. Hansma, Imaging soft samples with the atomic force microscope: gelatin in water and propanol, Biophys. J. 69 (1995) 264–270.
[18] M.E. Dokukin, I. Sokolov, On the measurements of rigidity modulus of soft materials in nanoindentation experiments at small depth, Macromolecules 45 (2012) 4277–4288.
[19] M.E. Harmon, D. Kuckling, C.W. Frank, Photo-cross-linkable PNIPAAm copolymers. 5. Mechanical properties of hydrogel layers, Langmuir 19 (2003) 10660–10665.
[20] K.D. Yao, W.G. Liu, Z. Lin, X.H. Qiu, In situ atomic force microscopy measurement of the dynamic variation in the elastic modulus of swollen chitosan/gelatin hybrid polymer network gels in media of different pH, Polym. Int. 48 (1999) 794–798.
[21] S. Ouasti, R. Donno, F. Cellesi, M.J. Sherratt, G. Terenghi, N. Tirelli, Network connectivity, mechanical properties and cell adhesion for hyaluronic acid/PEG hydrogels, Biomaterials 32 (2011) 6456–6470.
[22] J. Wiedemair, M.J. Serpe, J. Kim, J.-F. Masson, L.A. Lyon, B. Mizaikoff, C. Kranz, In-situ AFM studies of the phase-transition behavior of single thermoresponsive hydrogel particles, Langmuir 23 (2006) 130–137.
[23] C.A. Grant, P.C. Twigg, M.D. Savage, W.H. Woon, D. Greig, Mechanical investigations on agar gels using atomic force microscopy: effect of deuteration, Macromol. Mater. Eng. 297 (2012) 214–218.
[24] J.G. Jacot, S. Dianis, J. Schnall, J.Y. Wong, A simple microindentation technique for mapping the microscale compliance of soft hydrated materials and tissues, J. Biomed. Mater. Res. 79A (2006) 485–494.
[25] Y. Zhu, Z. Dong, U.C. Wejinya, S. Jin, K. Ye, Determination of mechanical properties of soft tissue scaffolds by atomic force microscopy nanoindentation, J. Biomech. 44 (2011) 2356–2361.
[26] S.S. Ng, C. Li, V. Chan, Experimental and numerical determination of cellular traction force on polymeric hydrogels, Interface Focus 1 (2011) 777–791.
[27] A.J. Engler, F. Rehfeldt, S. Sen, D.E. Discher, Microtissue elasticity measurements by atomic force microscopy and its influence on cell differentiation, in: D.E. Discher, Y.-L. Wang (Eds.), Methods in Cell Biology: Cell Mechanics, Elsevier, New York, NY, 2007, pp. 521–545.
[28] S. Ohya, S. Kidoaki, T. Matsuda, Poly(*N*-isopropylacrylamide) (PNIPAM)-grafted gelatin hydrogel surfaces: interrelationship between microscopic structure and mechanical property of surface regions and cell adhesiveness, Biomaterials 26 (2005) 3105–3111.
[29] D. Wang, S. Fujinami, K. Nakajima, S. Inukai, H. Ueki, A. Magario, T. Noguchi, M. Endo, T. Nishi, Visualization of nanomechanical mapping on polymer nanocomposites by AFM force measurement, Polymer 51 (2010) 2455–2459.
[30] Y. Sun, B. Akhremitchev, G.C. Walker, Using the adhesive interaction between atomic force microscopy tips and polymer surfaces to measure the elastic modulus of compliant samples, Langmuir 20 (2004) 5837–5845.
[31] S. Gupta, F. Carrillo, C. Li, L. Pruitt, C. Puttlitz, Adhesive forces significantly affect elastic modulus determination of soft polymeric materials in nanoindentation, Mater. Lett. 61 (2007) 448–451.
[32] J.C. Kohn, D.M. Ebenstein, Eliminating adhesion errors in nanoindentation of compliant polymers and hydrogels, J. Mech. Behav. Biomed. Mater. 20 (2013) 316–326.
[33] H.-J. Butt, B. Cappella, M. Kappl, Force measurements with the atomic force microscope: technique, interpretation and applications, Surf. Sci. Rep. 59 (2005) 1–152.

[34] A. Ganguly, A.K. Bhowmick, Quantification of surface forces of thermoplastic elastomeric nanocomposites based on poly(styrene-ethylene-*co*-butylene-styrene) and clay by atomic force microscopy, J. Appl. Polym. Sci. 111 (2009) 2104–2115.
[35] D.M. Panaitescu, Z. Vuluga, C. Radovici, C. Nicolae, Morphological investigation of PP/nanosilica composites containing SEBS, Polym. Test. 31 (2012) 355–365.
[36] D. Xu, K.M. Liechti, K. Ravi-Chandar, On the modified Tabor parameter for the JKR–DMT transition in the presence of a liquid meniscus, J. Colloid Interface Sci. 315 (2007) 772–785.
[37] C.A. Jones, Z.C. Grasley, J.A. Ohlhausen, Measurement of elastic properties of calcium silicate hydrate with atomic force microscopy, Cem. Concr. Compos. 34 (2012) 468–477.
[38] K. Daeinabi, M. Korayem, Indentation analysis of nano-particle using nano-contact mechanics models during nano-manipulation based on atomic force microscopy, J. Nanopart. Res. 13 (2011) 1075–1091.
[39] D.C. Lin, F. Horkay, Nanomechanics of polymer gels and biological tissues: a critical review of analytical approaches in the Hertzian regime and beyond, Soft Matter 4 (2008) 669–682.
[40] G.V. Lubarsky, M.R. Davidson, R.H. Bradley, Elastic modulus, oxidation depth and adhesion force of surface modified polystyrene studied by AFM and XPS, Surf. Sci. 558 (2004) 135–144.
[41] C.A. Clifford, M.P. Seah, Quantification issues in the identification of nanoscale regions of homopolymers using modulus measurement via AFM nanoindentation, Appl. Surf. Sci. 252 (2005) 1915–1933.
[42] M. VanLandingham, The effect of instrumental uncertainties on AFM indentation measurements, Microsc. Today 5 (1997) 12–15.
[43] M.R. VanLandingham, N.K. Chang, P.L. Drzal, C.C. White, S.H. Chang, Viscoelastic characterization of polymers using instrumented indentation. I. Quasi-static testing, J. Polym. Sci., B: Polym. Phys. 43 (2005) 1794–1811.
[44] D. Tranchida, S. Piccarolo, J. Loos, A. Alexeev, Mechanical characterization of polymers on a nanometer scale through nanoindentation. A study on pile-up and viscoelasticity, Macromolecules 40 (2007) 1259–1267.
[45] H. Hertz, Ueber die Berührung fester elastischer Körper, J. Reine Angew. Math. 1882 (1882) 156–171.
[46] S.K. Kaliappan, B. Cappella, Temperature dependent elastic–plastic behaviour of polystyrene studied using AFM force–distance curves, Polymer 46 (2005) 11416–11423.
[47] I.N. Sneddon, The relation between load and penetration in the axisymmetric Boussinesq problem for a punch of arbitrary profile, Int. J. Eng. Sci. 3 (1965) 47–57.
[48] B.V. Derjaguin, V.M. Muller, Y.P. Toporov, Effect of contact deformations on the adhesion of particles, J. Colloid Interface Sci. 53 (1975) 314–326.
[49] K.L. Johnson, K. Kendall, A.D. Roberts, Surface energy and the contact of elastic solids, Proc. R. Soc. London, Ser. A 324 (1971) 301–313.
[50] O. Piétrement, M. Troyon, General equations describing elastic indentation depth and normal contact stiffness versus load, J. Colloid Interface Sci. 226 (2000) 166–171.
[51] F. Piccinini, M. Levi, S. Turri, Photoactive sol–gel hybrid coatings from modified fluorocarbon polymers and amorphous titania, Prog. Org. Coat. 76 (2013) 1265–1272.
[52] C. Credi, S. Biella, C. De Marco, M. Levi, R. Suriano, S. Turri, Fine tuning and measurement of mechanical properties of crosslinked hyaluronic acid hydrogels as biomimetic scaffold coating in regenerative medicine, J. Mech. Behav. Biomed. Mater. 29 (2014) 309–316.
[53] J.E. Sader, J.W.M. Chon, P. Mulvaney, Calibration of rectangular atomic force microscope cantilevers, Rev. Sci. Instrum. 70 (1999) 3967–3969.
[54] B. Cappella, S.K. Kaliappan, H. Sturm, Using AFM force-distance curves to study the glass-to-rubber transition of amorphous polymers and their elastic–plastic properties as a function of temperature, Macromolecules 38 (2005) 1874–1881.
[55] W.C. Oliver, G.M. Pharr, An improved technique for determining hardness and elastic modulus using load and displacement sensing indentation experiments, J. Mater. Res. 7 (1992) 1564–1583.
[56] P.H. Mott, J.R. Dorgan, C.M. Roland, The bulk modulus and Poisson's ratio of incompressible materials, J. Sound Vib. 312 (2008) 572–575.
[57] Y.-T. Cheng, C.-M. Cheng, Relationships between initial unloading slope, contact depth, and mechanical properties for conical indentation in linear viscoelastic solids, J. Mater. Res. 20 (2005) 1046–1053.
[58] S. Tripathy, E.J. Berger, Measuring viscoelasticity of soft samples using atomic force microscopy, J. Biomech. Eng. 131 (2009) 094507.
[59] A.H.W. Ngan, H.T. Wang, B. Tang, K.Y. Sze, Correcting power-law viscoelastic effects in elastic modulus measurement using depth-sensing indentation, Int. J. Solids Struct. 42 (2005) 1831–1846.
[60] D. Passeri, A. Alippi, A. Bettucci, M. Rossi, E. Tamburri, M.L. Terranova, Indentation modulus and hardness of polyaniline thin films by atomic force microscopy, Synth. Met. 161 (2011) 7–12.
[61] J.D. Ferry, Viscoelastic Properties of Polymers, second ed., John Wiley & Sons, Inc., New York, NY, 1970.
[62] Y. Bautista, M.P. Gómez, C. Ribes, V. Sanz, Relation between the scratch resistance and the chemical structure of organic–inorganic hybrid coatings, Prog. Org. Coat. 70 (2011) 358–364.
[63] K. Terzaki, M. Kissamitaki, A. Skarmoutsou, C. Fotakis, C.A. Charitidis, M. Farsari, M. Vamvakaki, M. Chatzinikolaidou, Pre-osteoblastic cell response on three-dimensional, organic–inorganic hybrid material scaffolds for bone tissue engineering, J. Biomed. Mater. Res. A 101A (2013) 2283–2294.
[64] S. Akhlaghi, A. Sharif, M. Kalaee, A. Nouri, M. Manafi, Morphology, nanomechanical and thermodynamic surface characteristics of nylon 6/feather keratin blend films: an atomic force microscopy investigation, Polym. Int. 61 (2012) 646–656.
[65] R. Wagner, R. Moon, J. Pratt, G. Shaw, A. Raman, Uncertainty quantification in nanomechanical measurements using the atomic force microscope, Nanotechnology 22 (2011) 455703.